DOI: https://doi.org/10.24425/amm.2024.149767

MIN GYOO CHO[1], JAE HEE GO[1], BYUNG JOON CHOI[1*]

SIMPLIFYING HIGH-DENSITY MEMORY: EXPLOITING SELF-RECTIFYING RESISTIVE MEMORY WITH TiO_2/HfO_2 BILAYER DEVICES

Self-rectifying resistive memory can reduce the complexity of crossbar array architecture for high density memory. It can replace integrated memory and selector with one self-rectifying cell. Such a simple structure can be applied for the vertical resistive memory. Both top and bottom interface between insulating layer and electrodes are crucial to achieve highly self-rectifying memory cell. In this study, bilayer devices composed of HfO_2 and TiO_2 were fabricated using atomic layer deposition (ALD) for the implementation of self-rectifying memory cells. The physical, chemical, and electrical properties of HfO_2/TiO_2 and TiO_2/HfO_2 sandwiched between Pt and TiN electrodes were investigated. By analyzing the conduction mechanism of bilayer devices, the higher rectification ratio of TiO_2/HfO_2 stack was due to the difference in height and the number of energy barriers.

Keywords: Atomic layer deposition; bilayer; self-rectifying memory; rectification ratio

1. Introduction

With the progression of 4th industrial revolution, application of artificial intelligence and the Internet-of-Things are broadening, therefore, the necessity of faster information processing is ever increasing. In the Von Neumann architecture system, information is processed by the signal exchange between memory and central processing unit, which could result in so-called the memory-processor bottleneck [1,2]. Scaling or miniaturization has been progressed to increase the operation speed of complimentary MOS (CMOS) technology based semiconductor devices. However, scaling of CMOS technology and main memory, such as DRAM and flash memory, have reached the physical limits due to the charge-based information storage. To solve these problems, new nonvolatile memories and non-von Neumann computing architecture are actively studied so far [1,2].

Resistive random access memory (RRAM) is one of the new memories with non-volatile properties and fast operating speed. Unlike conventional memory, such as DRAM and flash memory, which store information based on charge, RRAM stores information by resistance state making it more advantageous in scaling. Its simple structure, metal-insulator-metal (MIM), makes it applicable to crossbar array architecture [3-5]. However, crossbar array architecture has a critical drawback, so called sneak current problem [6]. Integration of RRAM and the selector device (1S1R integrated device) can simply solve this problem; however, complex structure and complicated fabrication process are inevitable [3-6].

Self-rectifying memory cell (SRC) has a simple MIM structure, but functionally the same with 1S1R structure. It has a non-linear current-voltage (I-V) characteristics and resistively switching under forward direction and rectifying under reverse direction. Due to its nonlinearity and simple structure, the sneak current problem can be diminished, therefore, SRC has attracted a great interest as a computing memory and neuromorphic computing hardware [1,2].

In this study, we fabricated and evaluated the SRC with HfO_2/TiO_2 and TiO_2/HfO_2 stacks. Both HfO_2 and TiO_2 insulating layers are commonly used for active switching layer in RRAM. By changing the order of insulating layer, we tried to understand the origin of self-rectifying electrical property and its correlation with physical and chemical properties.

2. Experimental

HfO_2 and TiO_2 thin films for an SRC were grown by atomic layer deposition (ALD) [7,8]. TEMAHf ($C_{12}H_{32}HfN_4$) was used as the Hf precursor and TTIP ($C_{12}H_{28}O_4Ti$) was used as the Ti precursor. H_2O vapor was used as the reactant for both ALD

[1] SEOUL NATIONAL UNIVERSITY OF SCIENCE AND TECHNOLOGY, DEPARTMENT OF MATERIALS SCIENCE AND ENGINEERING, SEOUL 01811, KOREA

* Corresponding author: bjchoi@seoultech.ac.kr

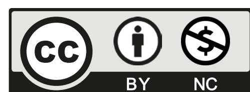

© 2024. The Author(s). This is an open-access article distributed under the terms of the Creative Commons Attribution-NonCommercial License (CC BY-NC 4.0, https://creativecommons.org/licenses/by-nc/4.0/deed.en which permits the use, redistribution of the material in any medium or format, transforming and building upon the material, provided that the article is properly cited, the use is noncommercial, and no modifications or adaptations are made.

processes. HfO_2 ALD was carried out at 250°C and TiO_2 ALD was carried out at 141°C in the different chamber. The HfO_2 ALD process was carried out 150 cycles for 15 nm target thickness with a 1s TEMAHF injection and a 30s N_2 purge followed by a 1s H_2O injection and a 30s N_2 purge. The TiO_2 ALD process was carried out 600 cycles for 20 nm target thickness with a 0.4s TTIP injection and a 30s N_2 purge followed by a 0.5s H_2O injection and a 30s N_2 purge. Each pulse sequence and time are optimized at the given deposition temperature and pressure conditions.

The thickness of deposited thin films was measured using Ellipsometer (Film Sense, FS-1) and high-resolution field emission scanning electron microscopy (FE-SEM, Hitachi High Technologies Corporation, Su8010). X-ray photoelectron spectroscopy (XPS, Nexsa, Al *Kα*) analyses were carried out to check the chemical properties of the film. For the device fabrication, HfO_2/TiO_2 and TiO_2/HfO_2 stack were deposited on the $TiN/SiO_2/Si$ substrate. Pt top electrode was deposited by sputtering using a dot-shaped shadow mask with a diameter of

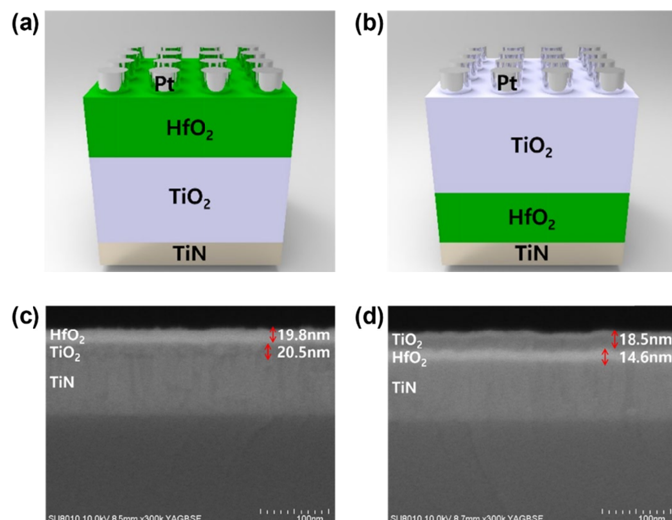

Fig. 1. Schematics of the fabricated device. (a) $Pt/HfO_2/TiO_2/TiN$ (PHTT) and (b) $Pt/TiO_2/HfO_2/TiN$ (PTHT). Cross-sectional scanning electron microscope images of (c) PHTT and (d) PTHT

100, 150, and 200 μm. Fabricated devices were analyzed using a semiconductor parameter analyzer (SPA, Hewlett-Packard, HP-4155A), Fig. 1 is the schematic diagram and FE-SEM images of fabricated devices of $Pt/HfO_2/TiO_2/TiN$ (PHTT) and $Pt/TiO_2/HfO_2/TiN$ (PTHT), respectively.

3. Results and discussion

Fig. 2 shows the depth profile of XPS spectra of the $HfO_2/TiO_2/TiN$ (HTT) and $TiO_2/HfO_2/TiN$ (THT) stacks. Ar^+ ion sputtering of 5 sec was carried 50 times for the depth profile. From the depth profile, the HfO_2 and TiO_2 layers of both stacks can be demarcated. Comparing Hf 4f spectra in a binding energy range of 13-25eV, peak shift to the lower angle at the surface of the HTT stack is found in Fig. 2(a). Comparing Ti 2p spectra, with a binding energy range of 454-468eV, Ti 2p spectra are visible in the HfO_2 area of the THT stack in Fig. 2(b). In addition, the higher binding energy of Hf 4f in THT stack can be found and thus $HfTiO_x$ phase exists in the THT stack. Therefore, considering the $HfTiO_x$ peak and Ti 2p spectra of the HfO_2 area of the THT stack, diffusion of Ti into HfO_2 layer underneath seems to occur during the deposition of TiO_2 on HfO_2 layer. This is due to the high reactivity of the TTIP precursor. Diffused Ti appears to bond with HfO_2 forming $HfTiO_x$ which may act as trap sites [9-11]. From Fig. 1(b), the thickness of the TiO_2 layer was similar in both stacks. However, the thickness of the HfO_2 layer was quite different. The substrate of the growing film clearly had an effect, but in this case, diffusion and reaction of TTIP with the HfO_2 layer could consume the pre-existing HfO_2, which could reduce the thickness of HfO_2 layer in PTHT.

Electrical properties of PHTT and PTHT devices were examined. Fig. 3 is the current density (*J*) – electric field (*E*) curves of PHTT and PTHT showing the conduction mechanisms under the range of electric field [12]. Both devices showed resistive switching and self-rectifying properties under positive bias applied on top of Pt electrode. However, rectifying ratio (between

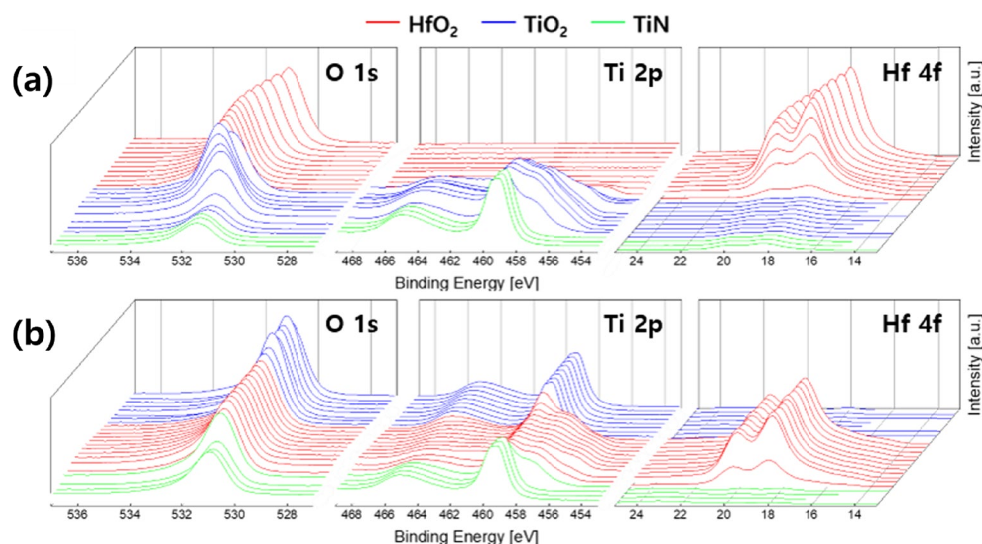

Fig. 2. XPS depth profile of (a) HTT and (b) THT stack

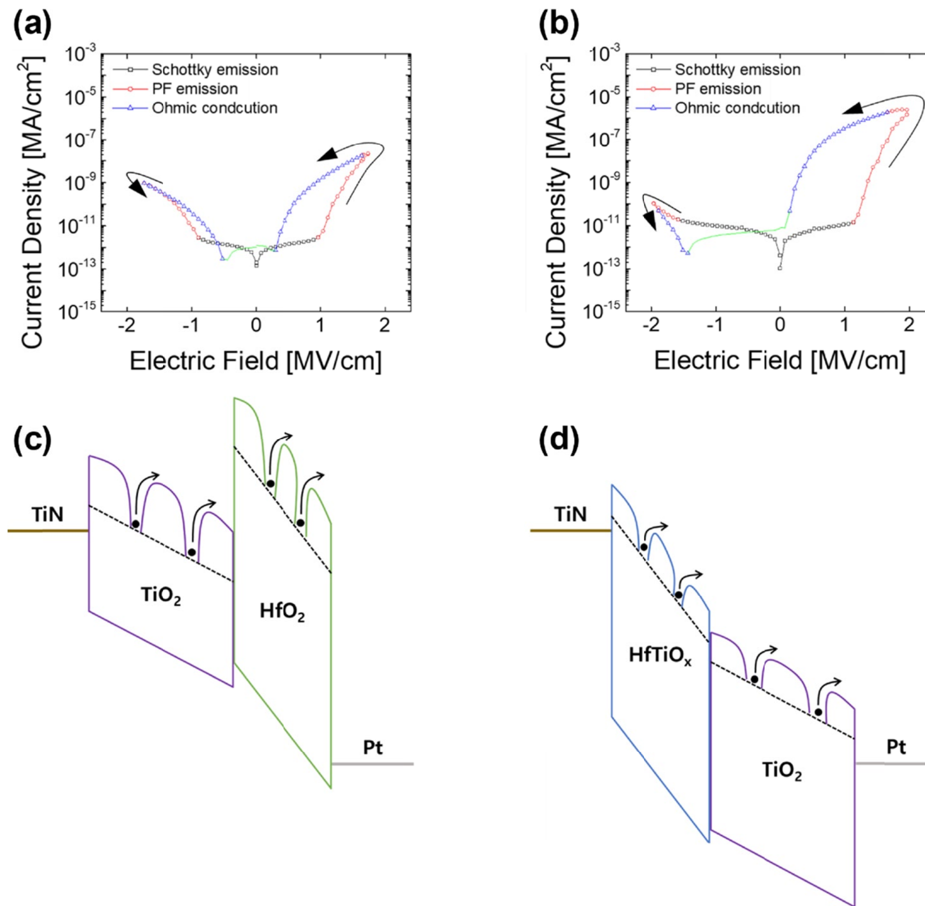

Fig. 3. *J-E* curves of (a) PHTT and (b) PTHT and their conduction mechanisms according to the electric field. Energy band diagram and plausible electron conduction of (c) PHTT and (d) PTHT

forward and reverse current) and the resistance ratio (between low-resistance and high-resistance under positive bias) can be different due to the barrier height and number of trap site in the bilayer [13,14]. The PHTT device showed a rectification ratio of 100 and the PTHT device showed a rectification ratio of 5000. The resistance ratio was 200 for PHTT and 1000 for PTHT. High rectifying ratio and resistance ratio are required for the crossbar array application. Therefore, it turns out that PTHT is superior than PHTT as an SRC. To explain the resistance hysteresis and self-rectifying behavior, the conduction mechanism and energy band diagram were considered.

As shown in Figs. 3(a) and 3(b), Schottky emission, Poole-Frankel (PF) emission, and Ohmic conduction were confirmed as the conduction mechanism [9]. After the Schottky emission at the lower electric field, PF emission is the dominating conduction mechanism under higher electric field. This means that once electrons overcome the Schottky barrier and then bulk-limited Pool-Frenkel conduction dominates in forward direction. The higher resistance ratio of PTHT compared to that of PHTT can be explained by the different trap energy levels and dielectric constant of each device. PTHT has a trap energy level of 0.7eV, while PHTT has a trap energy level of 1.25eV. PHTT has a higher trap energy level compared to that of PTHT, therefore, the current level is lower [15,16]. In addition, it appears that $HfTiO_x$ layer in PTHT can contain considerable amount of trap sites which can work as the conduction and resistive switching layer as well.

Figs. 3(c) and 3(d) represent simplified energy band diagrams for PHTT and PTHT devices. Bandgap energy of HfO_2 (4.72eV) and TiO_2 (3.2eV) dielectric layers and work function of TiN (4.5eV) and Pt (5.7eV) electrodes were considered. When positive bias voltage is applied on top Pt electrode for the PHTT device in Fig. 3(c), electrons have to go over the Schottky barrier of TiN/TiO_2 and TiO_2/HfO_2/ barrier subsequently. PF emission may occur once the electron overcomes such double barriers and penetrates through HfO_2 layer. On the contrary, when a positive bias is applied for the PTHT device, electrons have to go over the Schottky barrier of TiN/HfO_2 for the PF emission to occur as shown in Fig. 3(d). Once the electron overcome the Schottky barrier, PF emission occurs through the trap sites in HfO_2 layer. It is noted that there are plenty of trap sites due to the formation of $HfTiO_x$ in HfO_2 layer due to the diffused Ti inside the HfO_2 [10,16,17]. When a negative bias is applied on PTHT device, electrons have to go over the double barriers of Pt/TiO_2 and TiO_2/HfO_2 barrier to reach the TiN bottom electrode, therefore, high rectification ratio is expected. In other words, the PHTT device has a lower rectification ratio because of the number of barriers and barrier height under positive and negative bias; electrons have to go over double barriers and go through the PF trap sites under positive bias, while Schottky barrier of single Pt/HfO_2 should be overcome under negative bias.

4. Conclusions

ALD-grown HfO_2 and TiO_2 bilayer devices with HfO_2/TiO_2 (HTT) and TiO_2/HfO_2 (THT) stacks on TiN bottom electrode were fabricated and compared for the implementation of SRC. From the XPS depth profile analysis, it was confirmed that the stack difference led by the diffusion of Ti into HfO_2 layer below in the THT stack during the deposition of TiO_2, while rather cleaner interface formed between HfO_2/TiO_2 in HTT stack. Both devices showed self-rectifying behavior and resistance-switching hysteresis, but higher rectification ratio and resistance ratio were observed in PTHT device. From the analysis of conduction mechanism, Schottky and PF emission were confirmed as the main conduction mechanism under the low and high electric field, respectively. Main difference was considered that lower Schottky barrier of TiN/TiO_2 and diffused Ti inside the HfO_2 of the PTHT stack acted as trap sites, which makes PTHT device more conductive under positive bias regime. SRC device of PTHT with higher rectification and resistance ratio could be applied to crossbar array for the high density memory and synaptic device for neuromorphic computing in the future. However, poor retention property of PTHT and PHTT devices should be remedied.

Acknowledgment

This work was supported by the National Research Foundation of Korea (NRF) grant funded by the Korea government (MSIT) (Grant No. 2022M3F3A2A01044952).

REFERENCES

[1] S. Choi, Y. Kim, T. van Nguyen, W.H. Jeong, K.S. Min, B.J. Choi, Low-Power Self-Rectifying Memristive Artificial Neural Network for Near Internet-of-Things Sensor Computing. Adv. Electron. Mater. **7** (6), 2100050 (2021). DOI: https://doi.org/10.1002/aelm.202100050

[2] Q. Luo, X. Zhang, Y. Hu, T. Gong, X. Xu, P. Yuan, H. Ma, D. Dong, H. Lv, S. Long, Q. Liu, M. Liu, Self-Rectifying and Forming-Free Resistive-Switching Device for Embedded Memory Application. IEEE Electron Device Lett. **39** (5), 664-667 (2018). DOI: https://doi.org/10.1109/LED.2018.2821162

[3] H. Ryu, S. Kim, Self-Rectifying Resistive Switching and Short-Term Memory Characteristics in Pt/HfO_2/TaO_x/TiN Artificial Synaptic Device. Nanomater. **10** (11), 159 (2020). DOI: https://doi.org/10.3390/nano10112159

[4] K.V. Pham, T.V. Nguyen, S.B. Tran, H.K. Nam, M.J. Lee, B.J. Choi, S.N. Truong, K.S. Min, Memristor Binarized Neural Networks. J. Semicond. Technol. Sci. **18** (5), 568-577 (2018). DOI: https://doi.org/10.5573/JSTS.2018.18.5.568

[5] N.K. Upadhyay, W. Sun, P. Lin, S. Joshi, R. Midya, X. Zhang, Z. Wang, H. Jiang, J.H. Yoon, M. Rao, M. Chi, Q. Xia, J. Yang, A Memristor with Low Switching Current and Voltage for 1S1R Integration and Array Operation. Adv. Electron. Mater. **6**, 1901411 (2020). DOI: https://doi.org/10.1002/aelm.201901411

[6] Y. Kim, W.H. Jeong, S.B. Tran, H.C. Woo, J. Kim, C.S. Hwang, K.S. Min, B.J. Choi, Memristor crossbar array for binarized neural networks. AIP Adv. **9** (4), 045131 (2019). DOI: https://doi.org/10.1063/1.5092177

[7] J.Y. Park, Y.B. Won, M.J. Jeong, B.J. Choi, Structural, Electrical, and Optical Properties of ZnO Films Grown by Atomic Layer Deposition at Low Temperature. Arch. Metall. Mater. **67** (4), 1503-1506 (2022). DOI: https://doi.org/10.24425/amm.2022.141082

[8] H.J. Yun, S.Y. Ryu, H.Y. Lee, W.Y. Park, S.G. Kim, B.J. Choi, Multilevel Operation of GdO_x-Based Resistive Switching Memory Device Fabricated by Post-Deposition Annealing. Ceram. Inter. **47** (12), 16597-16602 (2019). DOI: https://doi.org/10.1016/j.ceramint.2021.02.231

[9] J.H. Yoon, D.E. Kwon, Y.J. Kwon, K.J. Yoon, T.H. Park, X.L. Shao, C.S. Hwang, The Current Limit and Self-Rectification Functionalities in the TiO_2/HfO_2 Resistive Switching Material System. Nanoscale **9** (33), 11920 (2017). DOI: https://doi.org/10.1039/c7nr0221Sh

[10] J.H. Ryu, S. Kim, Artificial Synaptic Characteristics of TiO_2/HfO_2 Memristor with Self-Rectifying Switching for Brain-Inspired Computing. Chaos Solit. Fractals **140**, 110236 (2020). DOI: https://doi.org/10.1016/j.chaos.2020.110236

[11] H. Hernandez-Arriaga, E. Lopez-Luna, E. Martinez-Guerra, M.M. Turrubiartes, A.G. Rodriguez, M.A. Vidal, Growth of HfO_2/TiO_2 Nanolaminates by Atomic Layer Deposition and HfO_2-TiO_2 by Atomic Partial Layer Deposition. J. Appl. Phys. **121** (6), 064302 (2017). DOI: https://doi.org/10.1063/1.4975676

[12] F.C. Chiu, A Review on Conduction Mechanism in Dielectric Films, Adv. Mater. Sci. Eng. 2014, 578168 (2014). DOI: https://doi.org/10.1155/2014/578168

[13] Y. Kim, M.S. Kim, H.J. Yun, S.Y. Ryu, B.J. Choi, Effect of growth temperature on AlN thin films fabricated by atomic layer deposition. Ceram. Inter. **44** (14), 17447 (2018). DOI: https://doi.org/10.1016/j.ceramint.2018.06.212

[14] S. Choi, A.S. Ansari, H.J. Yun, H. Kim, B. Shong, B.J. Choi, Growth of Al-rich AlGaN thin films by purely thermal atomic layer deposition. J. Alloy Comp. **854**, 157186 (2021). DOI: https://doi.org/10.1016/j.jallcom.2020.157186

[15] J.H. Yoon, S.J. Song, I.H. Yoo, J.Y. Seok, K.J. Yoon, D.E. Kwon, T.H. Park, C.S. Hwang, Highly Uniform, Electroforming-Free, and Self-Rectifying Resistive Memory in the Pt/Ta_2O_5/HfO_{2-x}/TiN Structure. Adv. Funct. Mater. **24** (32), 5086-5095 (2014). DOI: https://doi.org/10.1002/adfm.201400064

[16] C.W. Hsu, T.H. Hou, M.C. Chen, I.T. Wang, C.L. Lo, Bipolar Ni/TiO_2/HfO_2/Ni RRAM With Multilevel States and Self-Rectifying Characteristics. IEEE Electron Device Lett. **34** (7), 885-887 (2013). DOI: https://doi.org/10.1109/LED.2013.2264823

[17] H. Ma, J. Feng, H. Lv, T. Gao, X. Xu, Q. Luo, T. Gong, P. Yuan, Self-Rectifying Resistive Switching Memory with Ultralow Switching Current in Pt/Ta_2O_5/HfO_{2-x}/Hf Stack. Nanoscale Res. Lett. **12** (1), 118 (2017). DOI: https://doi.org/10.1186/s11671-071-1905-3